Available online at www.sciencedirect.com
SCIENCE DIRECT®
International Journal of Mass Spectrometry 241 (2005) 57–61
International Journal of Mass Spectrometry
www.elsevier.com/locate/ijms

Multiple secondary ion emission from keV massive gold projectile impacts

R.D. Rickman[a], S.V. Verkhoturov[a], G.J. Hager[a], E.A. Schweikert[a,*], J.A. Bennett[b]

[a] *Department of Chemistry, Texas A&M University, College Station, TX 77842-3012, USA*
[b] *International SEMATECH, Austin, TX 78741, USA*

Received 12 July 2004; accepted 12 October 2004
Available online 30 November 2004

Abstract

We present the first experimental data on secondary ion emission characteristics from the impact of 26 keV Au_3^+ and 74.6–114.6 keV Au_{400}^{4+}. In particular we show secondary ion yield distributions and secondary ion and coincidental ion yields of molecular cluster ions from single impact events. The target consisted of an amorphous $(HfO_2)_{0.6}(SiO_2)_{0.4}$ layer deposited on a Si wafer. Large increases in higher order emission events and both secondary ion and coincidental ion yields within these events were observed for bombardment with Au_{400}^{4+} even though the energy per atom of this projectile is more than an order of magnitude less than Au_3^+.

Keywords: Secondary ion emission; Yield distributions; Gold projectile impacts; Coincidental ion yield

1. Introduction

A key factor affecting the performance of secondary ion mass spectrometry (SIMS) as a surface analytical tool is the effectiveness of the bombarding projectile to generate secondary ions [1,2]. A useful approach for increasing the secondary ion yield is to bombard with polyatomic instead of atomic projectiles, as documented in studies involving, for example, the secondary ions produced from Au_n^+ ($1 \leq n \leq 9$) or C_{60}^+ impacts [3–6]. Data from more massive projectiles are sparse. They show promising trends: molecular ion yields and the ratio of molecular-to-fragment ions increase as the size of the bombarding cluster increases [8,9]. A recent study with 40 keV Au_{400}^{4+} suggests that the analytical signal increases faster than the damage cross-section, i.e. the volume of sample destroyed per projectile impact [10]. The present study further examines Au_{400}^{4+} as a projectile for SIMS. The experiments were run in the event-by-event bombardment detection mode, i.e. the bombardment amounts to successive individual Au_{400}^{4+} impacts each resolved in time and space. The data acquisition scheme was designed to record each impact and any resulting secondary ions individually. With this approach we could identify and quantify "multi-ion events", i.e. the emission of multiple secondary ions from single projectile impacts.

The inventory of the types of emission events is of interest to address fundamental questions on the desorption–ionization processes involved in low velocity Au_{400}^{4+} impacts. In the context of SIMS, multi-ion events hold promise for the analysis of nano-domains since co-emitted secondary ions must originate from molecules located together within the surface volume perturbed by a single projectile [11]. The relevance for analysis of nano-structures will depend on the effectiveness of Au_{400}^{4+} to cause co-emission of two or more analytically significant secondary ions. We present below the first experimental data on multi-ion emission from Au_{400}^{4+}. Data on similar types of emission events obtained with Au_3^+ bombardment are included for comparison.

* Corresponding author. Tel.: +1 979 845 2341; fax: +1 979 845 1655.
E-mail address: schweikert@mail.chem.tamu.edu (E.A. Schweikert).

1387-3806/$ – see front matter © 2004 Elsevier B.V. All rights reserved.
doi:10.1016/j.ijms.2004.10.009

2. Experimental

2.1. Instrumentation

A schematic of the instrument is given in Fig. 1. Gold primary ions were produced using a liquid metal ion source (LMIS) described elsewhere [2]. Briefly, a reservoir and needle assembly, filled with an Au/Si eutectic, is heated. Once the eutectic melts, and a critical extraction voltage is applied, ion formation occurs at the tip of the needle, creating Au_n^+ ions. Recent experiments with this source have shown that, under certain conditions, higher mass clusters can be extracted that have a mass-to-charge ratio of approximately 20,000 [12]. Under these conditions, it was determined that, on average, each cluster contained 400 atoms with an overall net charge of +4 on the cluster. The initial kinetic energy of the primary ions could be adjusted from +10 to +20 keV.

The extracted current was focused with a series of electrostatic lenses into a Wien filter. The Wien filter allows a projectile with a particular velocity to pass while deflecting all others. All of these experiments were conducted in the event-by-event bombardment/detection mode. The primary concern is that the detected secondary ions are ejected from the impact of a *single* projectile. To meet this requirement the filtered beam is passed between a set of high voltage deflection plates, pulsed between +1 and −1 kV at 10 kHz, to reduce the intensity of the primary ion beam. The beam then passes through a 0.4 mm aperture before reaching the target. Through a combination of defocusing, pulsing, and using apertures, we are able to meet the condition of single projectile impacts with an average of 0.1 primary ions per pulse.

For all experiments the target potential was kept at a constant −8.6 kV. Secondary electrons, from the impact of the primary ion, are steered by a weak magnetic field to a chevron array micro-channel plate (MCP) detector generating a start signal for a time-of-flight mass spectrum of any secondary ions created by that particular primary ion. The secondary ions are accelerated towards a drift tube (60 cm) where they then separate, based on the square root of their mass-to-charge, before striking an eight-anode MCP detector array. The multi-anode detector assembly consists of two MCPs with a 25 mm active area in a chevron configuration. The multi-anode detector is located 2 mm from the last MCP. The detector is manufactured from a copper coated circuit board with eight equivalent pie-shaped anodes etched onto the circuit board. The eight anodes are separated from each other by a 1.5 mm gap separated by ground. This design minimizes cross-talk between adjacent anodes. The degree of cross-talk was tested by masking non-adjacent anodes. In this configuration no signal from the masked anodes should be recorded. When the counts on each anode were examined, the degree of cross-talk between the exposed and masked anodes was less than 0.1%. The total transmission/detection efficiency for secondary ions is estimated to be ∼0.3, as a product of three efficiencies: transmission of the grids (0.73), active surface of the MCP (0.50), and active area of the multi-anode (0.8). The signal from each detector is converted into a logic pulse by a constant fraction discriminator (CFD) before being passed through a fast time-to-digital converter, TDC (CTN-M4 Orsay Electronics).

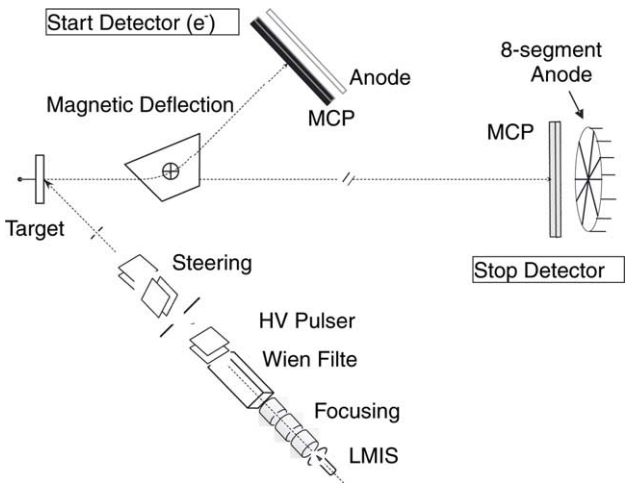

Fig. 1. Schematic of To-SIMS instrument with LMIS and eight-anode secondary ion detector.

2.2. Measurement

As mentioned earlier, each experiment is carried out in the event-by-event mode at the limit of single ion impacts. An event is described as the interaction of the primary ion with the target. This interaction can result in the ejection of secondary ions or neutrals. For these experiments we detect only the secondary ions. In practice the number of secondary ions ejected by a single projectile is statistically insignificant, to overcome this obstacle many (10^6–10^7) single projectile impact events are recorded. From this number of events it is possible to generate information that is statistically representative of the sample.

Data are acquired in what is termed as the total matrix of events mode [7]. More specifically, the arrival of the secondary electron at the start detector signals the start of the first event, E_1. Secondary ions, created in E_1, are accelerated towards the eight-anode stop detector. The arrival time of secondary ion 1 from event 1, SI_1^1, is recorded by a time-to-digital converter (TDC). The arrival times of co-emitted secondary ions, up to the last from this event, SI_1^k, are recorded, and then passed to the data acquisition computer. The variable k is the total number of detected ions from that event. This process is then repeated for the next event, E_2, through the last recorded event, E_n, with each k-ion emission event stored as an additional row in its respective array.

2.3. Sample

The sample, provided by International SEMATECH, consisted of a mixture of 40% SiO_2 and 60% HfO_2 deposited as

an amorphous layer approximately 4 nm thick on a Si wafer. The complex composition provided multiple secondary ions of both homogeneous Hf and Si oxides and heterogeneous HfSi oxides.

3. Results and discussion

3.1. Mass spectra

The total matrix of events data acquisition mode coupled with the eight-anode detector allows for the recording of up to eight identical ions, from the same event, provided they strike different anodes. Fig. 2 shows a mass spectrum of negative ions from 74.6 keV $Au_{400}{}^{4+}$ bombardment of the $(HfO_2)_{0.6}(SiO_2)_{0.4}$ sample. This spectrum consists of secondary ions accumulated from $\sim 2 \times 10^7$ primary ion impacts. The spectrum shows heterogeneous and homogeneous clusters of HfO_2 and SiO_2. Also present are peaks for Au^- and $Au_2{}^-$. Although not shown, a peak for $Au_3{}^-$ was also observed. The presence of gold in the spectrum is attributed to reflection of gold atoms from the projectile [10]. The same targets were also examined with 26 keV $Au_3{}^+$. In this case there was no visible peak for this cluster ion.

3.2. Secondary ion yields

One measure of the efficiency of a projectile is the secondary ion yield. The secondary ion yield for ion i (e.g. $SiO_2{}^-$), Y_i, is defined as:

$$Y_i = \sum_k Y_i(k) = \sum_k \frac{I_i(k)}{N} \quad (1)$$

where $Y_i(k)$ and $I_i(k)$ are the yield and the number of detected secondary ions, respectively, for ion i in k-ion emission events, and N is the total number of events. Fig. 3 is a plot of the secondary ion yields of various secondary ions as

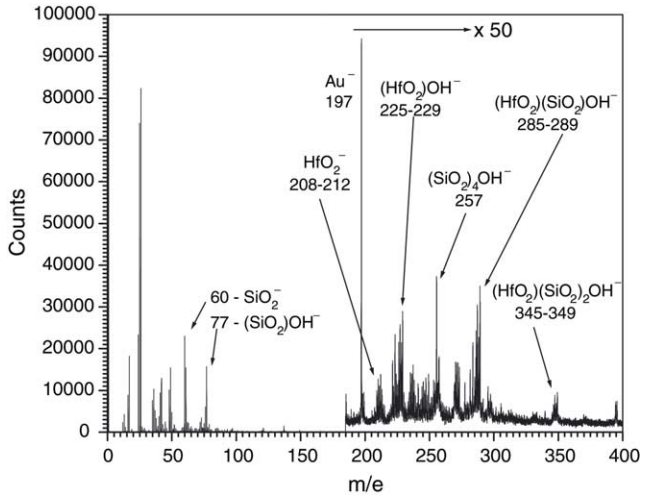

Fig. 2. Negative ion mass spectrum from 74.6 keV $Au_{400}{}^{4+}$ bombardment of an amorphous $HfSiO_x$ target.

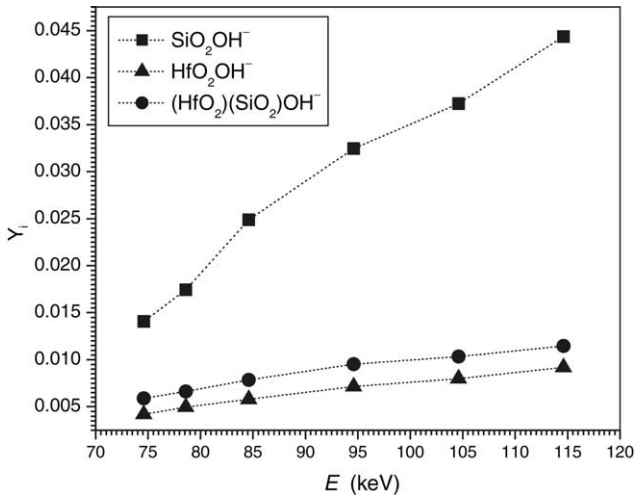

Fig. 3. Secondary ion yields, Y_i, as a function of the primary ion ($Au_{400}{}^{4+}$) kinetic energy for the indicated cluster ions. The margins of error in the values of Y_i are less than ±2%. Lines are to guide the eye.

a function of projectile kinetic energy, E. There is a linear dependency of yields versus energy in this range. Note that projectile energy increases by a factor of 1.6, but secondary ion yields for SiO_2OH^- increase by a factor of 3 and by a factor of ~2 for the other two secondary ions.

The more pronounced dependency of the SiO_2OH^- yield on E may be explained by considering the source of the SiO_2. A further comment can be made about the depth of emission. Bombardment of HfO_2 layers having thickness from 2 to 20 nm on silicon substrates shows that the Hf- and Si-containing secondary ions are emitted from depths of up to 10 nm [13]. The depth of secondary ion emission exceeds the range of an equal velocity Au^+ projectile, due perhaps to high energy density deposition. With that information one can consider two contributions to the yield of SiO_2OH^-. One is from the deposited mixture of Hf and Si oxides (4 nm in thickness), the other comes from the interfacial SiO_2 layer on the Si substrate. As the energy of the projectile increases so does the contribution of SiO_2 from the interfacial SiO_2 layer. This results in inflated yields for this secondary ion due to changing stoichiometry in the volume perturbed by the projectile.

This prompts the question to what extent "multi-ion events" contribute to these yields. To address this, the overall secondary ion yield, Y_i, can be separated into two subsets, one is $Y(k = 1)$ and the other is $Y(k \geq 2)$ corresponding to single ion emission events and multiple ion emission events or "multi-ion events". Fig. 4 is a plot of the yield of SiO_2OH^- for these two types of events. For this ion the yields increase with E, however after about 80 keV the "multi-ion events" begin to become more productive with respect to the emission of this ion and at 114 keV they are over twice as efficient for production of SiO_2OH^-. Figs. 5 and 6 are similar plots for HfO_2OH^- and the heterogeneous cluster $(HfO_2)(SiO_2)OH^-$. Similar trends are present for these two analytically significant secondary ions.

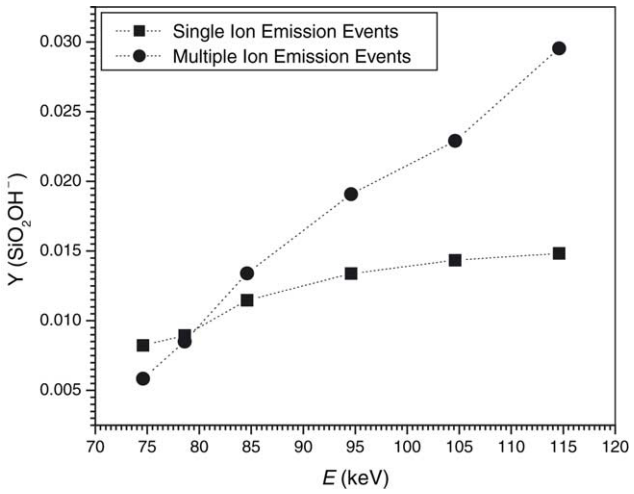

Fig. 4. Secondary ion yields for SiO_2OH^- from single and multiple secondary ion emission events as a function of primary ion (Au_{400}^{4+}) kinetic energy. The margins of error in the values of $Y(SiO_2OH^-)$ are less than ±2%. Lines are to guide the eye.

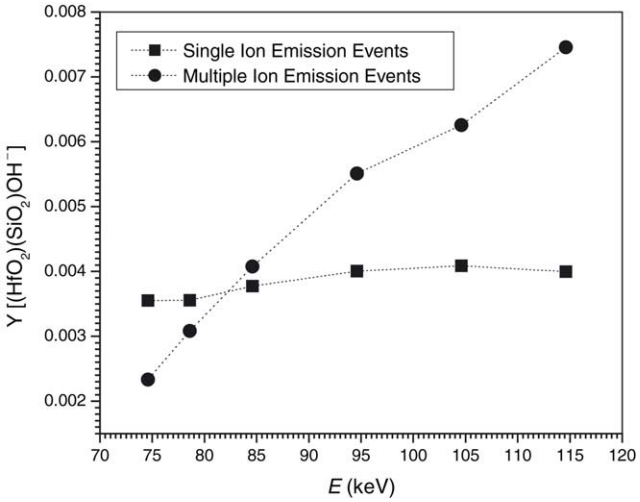

Fig. 6. Secondary ion yields for the heterogeneous cluster $(HfO_2)(SiO_2)OH^-$ from single and multiple secondary ion emission events as a function of primary ion (Au_{400}^{4+}) kinetic energy. The margins of error in the values of $Y((HfO_2)(SiO_2)OH^-)$ are less than ±2%. Lines are to guide the eye.

3.3. Coincidental ion yields

These are multiple secondary ion emission events. The yield of co-emitted ions *i* and *j*, Y_{ij}, is defined as:

$$Y_{ij} = \sum_k Y_{ij}(k) = \sum_k \frac{I_{ij}(k)}{N} \quad (2)$$

where $Y_{ij}(k)$ and $I_{ij}(k)$ are the yield and number of co-emitted ions detected, respectively, for ions *i* and *j*. Fig. 7 is a plot of these yields for two sets of secondary ions. The first set comprises the yields for cases where $(SiO_2)OH^-$ is co-emitted with $(HfO_2)OH^-$ and the second set comprises the yields for cases where $(SiO_2)OH^-$ is co-emitted with $(HfO_2)(SiO_2)OH^-$. The coincidental ion yields increase by a factor of ∼4 and ∼5, respectively, over the energy range. This increase is almost twice of that observed in the secondary ion yields for these ions.

Fig. 8 is a plot of the yields of SiO_2OH^- as a function of *E* for cases where two or three of these ions were detected from the impact of a single projectile. In both cases there is a linear dependency of the yields as a function of *E*. The slope of the lines begins to deviate at $E > 95$ keV with the case where three SiO_2OH^- ions are detected changing more rapidly.

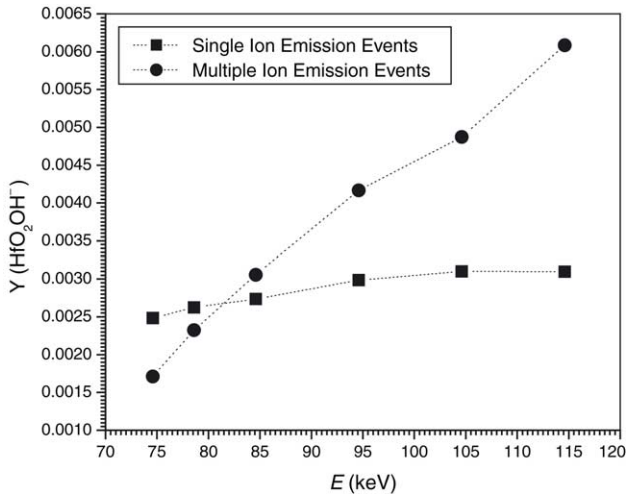

Fig. 5. Secondary ion yields for HfO_2OH^- from single and multiple secondary ion emission events as a function of primary ion (Au_{400}^{4+}) kinetic energy. The margins of error in the values of $Y(HfO_2OH^-)$ are less than ±2%. Lines are to guide the eye.

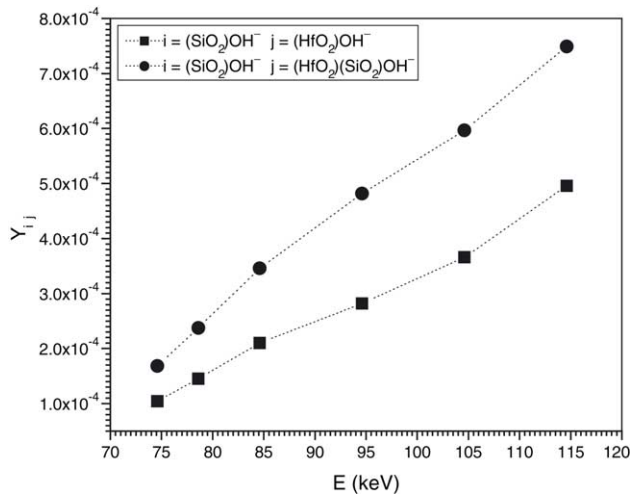

Fig. 7. Coincidental secondary ion yields, Y_{ij}, as a function of primary ion (Au_{400}^{4+}) kinetic energy for the selected ion combinations. The margins of error in the values of Y_{ij} are less than ±2%. Lines are to guide the eye.

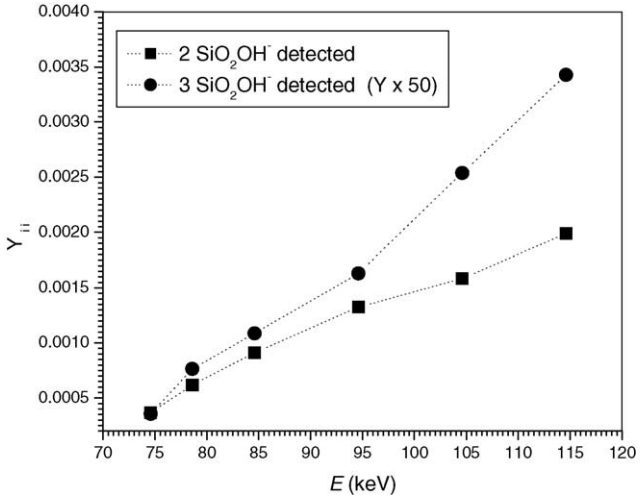

Fig. 8. Coincidental secondary ion yields, Y_{ii}, as a function of primary ion ($Au_{400}{}^{4+}$) kinetic energy for SiO_2OH^- for cases where two or three ions were detected. The margins of error in the values of Y_{ii} are less than ±2%. Lines are to guide the eye.

3.4. Ion yield distributions

Individual events differ in the number, *k*, and type of secondary ions, *i*, that are detected. One can examine the frequency of occurrence of "multi-ion events" for a given projectile energy in the form of the total ion yield distribution $Y(k) = \sum_i Y_i(k)$. Fig. 9 is a plot of the total ion yield distribution for bombardment by $Au_{400}{}^{4+}$ as a function of *k*, at the indicated bombardment energy. There is little increase in the frequency of occurrence of events in which a single ion is detected for this energy range. If one examines the events in which multiple secondary ions were detected the trends differ. For example, for events in which five secondary ions were detected the yield increases by over an order of magnitude as the impact energy increases. There are more cases of multiple secondary ion emission for the highest energy $Au_{400}{}^{4+}$ than there are single ion emission events. For reference, multi-ion emission data for 26.2 keV $Au_3{}^+$ bombardment are also shown. The effectiveness of $Au_{400}{}^{4+}$ for producing multiple secondary ion emission is clearly evident.

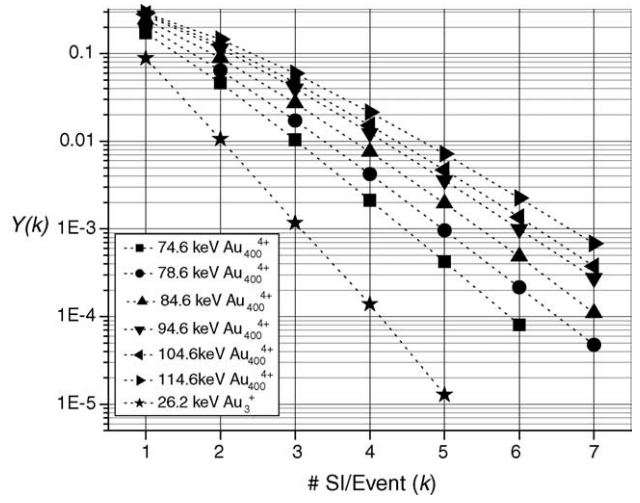

Fig. 9. Total ion yield distributions $Y(k)$ for $Au_{400}{}^{4+}$ bombardment of the $HfSiO_x$ target at the indicated energies. This distribution from 26.2 keV $Au_3{}^+$ bombardment is plotted for comparison. The margins of error in the values of $Y(k)$ are less than ±2%. Lines are to guide the eye.

4. Conclusions

Massive projectiles such as Au_{400} can expand the scope of SIMS. To gain some insight into how their impact translates into the emission of secondary ions, we have applied a novel method to investigate the collision cascade. A key finding is the preponderance of multi-ion events with increasing projectile energy. A further surprising observation is that the analyte specific secondary ions originate from depths of several nm. Thus, Au_{400} offers, via the secondary ions emitted in multi-ion events, a means for probing nano-environments truly within a solid.

Acknowledgements

This study was funded by the NSF (CHE-0135888) and the R.A. Welch Foundation (A-1482).

References

[1] M.G. Blain, S. Della-Negra, H. Joret, Y. Le Beyec, E.A. Schweikert, Phys. Rev. Lett. 63 (1989) 1625.
[2] M. Benguerba, A. Brunelle, S. Della-Negra, J. Depauw, H. Joret, Y. Le Beyec, M.G. Blain, E.A. Schweikert, G. Ben Assayag, P. Sudraud, Nucl. Instrum. Meth. B 62 (1991) 8.
[3] R.D. Rickman, S.V. Verkhoturov, E.S. Parilis, E.A. Schweikert, Phys. Rev. Lett. 92 (2004) 47601.
[4] S. Bouneau, A. Brunelle, S. Della-Negra, J. Depauw, D. Jacquet, Y. Le Beyec, M. Pautrat, M. Fallavier, J.C. Poizat, H.H. Andersen, Phys. Rev. B 65 (2002) 144106.
[5] J. Xu, S. Ostrowski, C. Szakal, A.G. Ewing, N. Winograd, Appl. Surf. Sci. 231/232 (2004) 159.
[6] D.E. Weibel, N. Lockyer, J.C. Vickerman, Appl. Surf. Sci. 231/232 (2004) 146.
[7] R.D. Rickman, Secondary Ion Emission from "Super-Efficient" Events: Prospects for Surface Mass Spectrometry, Ph.D. Dissertation, Texas A&M University, College Station, Texas, 2004, p. 37.
[8] J.F. Mahoney, E.S. Parilis, T.D. Lee, Nucl. Instrum. Meth. B 88 (1994) 154.
[9] R.A. Zubarev, I.S. Bitensky, P.A. Demirev, B.U.R. Sundqvist, Nucl. Instrum. Meth. B 88 (1994) 143.
[10] A. Tempez, J.A. Schultz, S. Della-Negra, J. Depauw, D. Jacquet, A. Novikov, Y. Lebeyec, M. Pautrat, M. Caroff, M. Ugarov, H. Bensaoula, M. Gonin, K. Fuhrer, A. Woods, Rapid Commun. Mass Spectrometr. 18 (2004) 371.
[11] S.V. Verkhoturov, E.A. Schweikert, N.M. Rizkalla, Langmuir 18 (2002) 8836.
[12] S. Bouneau, S. Della-Negra, J. Depauw, D. Jacquet, Y. Le Beyec, J.P. Mouffron, A. Novikov, M. Pautrat, Nucl. Instrum. Meth. B 225 (2004) 579.
[13] R.D. Rickman, S.V. Verkhoturov, G.J. Hager, E.A. Schweikert, J.A. Bennett, Abstracts of the 17th Annual Workshop on SIMS, Westminster, CO, 2004.